PERGAMON

International Journal of Heat and Mass Transfer 43 (2000) 3823–3834

International Journal of HEAT and MASS TRANSFER

www.elsevier.com/locate/ijhmt

Simulation of vertical slot convection using 'one-dimensional turbulence'

Thomas D. Dreeben[a,*], Alan R. Kerstein[b]

[a]Osram Sylvania, 71 Cherry Hill Drive, Beverly, MA 01915, USA

[b]Combustion Research Facility, Sandia National Laboratories, Livermore, CA 94551-0969, USA

Received 8 June 1999; received in revised form 10 December 1999

Abstract

One-dimensional turbulence (ODT) is used to model and simulate the buoyant turbulent flow in a vertical slot. ODT reproduces available Direct Numerical Simulation results on the Rayleigh number dependence of wall heat transfer and of other flow properties of interest. Extended ranges of Rayleigh and Prandtl numbers are investigated with ODT to explore the broader behavior of the flow, focusing on its connection to classical scaling arguments. Published by Elsevier Science Ltd.

1. Introduction

One-dimensional turbulence (ODT) is a recent development in turbulence modeling, which has been shown to apply to various turbulent flow configurations. These include [1–4] homogeneous turbulence, boundary layers, Couette flow, temporal jets, shear layers, Rayleigh convection, and combustion in the turbulent-jet diffusion flame. In this work, we extend the applicability of the model to include buoyant convection in a vertical slot. It has been noted [5] that the dynamics of this flow differ from those of Rayleigh–Bénard convection, because the statistical inhomogeneity is aligned perpendicular to the direction of the buoyant force. The recent availability of experimental data [6,7] and of Direct Numerical Simulation (DNS) data [5,8] on this problem permits useful comparisons of scaling properties of the model.

Establishing credibility by reproducing known results in turbulent flows is a common objective of turbulence modeling efforts. A less common objective is to shed light on unknown aspects of turbulence in flows of either scientific or engineering significance [9]. In addition to comparison with known DNS results, ODT is used here to assess the applicability of basic scaling arguments to the Rayleigh number dependence of physical quantities such as the heat transfer and the peak mean velocity. A study of such relationships over a range of Prandtl numbers in ODT sheds new light on which flow parameters are most important in the scaling behavior.

2. Problem description

The problem considered here is vertical slot convection as shown in Fig. 1, in which buoyant fluid flows between two infinite parallel walls. The flow is driven by a temperature difference $\Delta T = T_1 - T_2$, imposed as a Dirichlet boundary condition across two vertical walls which are separated by a distance h. The profile of temperature T generates a buoyant momentum source through the Boussinesq approximation. This

* Corresponding author.

0017-9310/00/$ - see front matter Published by Elsevier Science Ltd.
PII: S0017-9310(00)00012-0

Nomenclature

A	ODT model constant
C_f	friction coefficient
E	eddy triplet map
L_{max}	location of the maximum mean velocity
M_{dt}	eddy-based momentum flux
Nu	Nusselt number $= q_w h/(\kappa\Delta T)$
P	pressure
Pr	Prandtl number $= \nu/\kappa$
Q	flux of arbitrary property ϕ
Ra	Rayleigh number $= g\beta\Delta T h^3/(\kappa\nu)$
Re	Reynolds number
T_1	left wall temperature
T_2	right wall temperature
ΔT	$T_1 - T_2$
T	local temperature
T_c	mean centerplane temperature
T_{ref}	reference temperature
$\bar{T}$	bulk temperature
W_{max}	maximum mean velocity
g	magnitude of the acceleration due to gravity
h	slot width
l	eddy size
t	time
q_w	wall heat transfer
x	cross-stream coordinate
x_0	location of an eddy's left endpoint
w	streamwise velocity
$[\frac{\partial w}{\partial x}]_{eddy}$	eddy velocity gradient
z	streamwise coordinate

Greek symbols

β	thermal expansion coefficient
η	normalized position within an eddy
κ	thermal diffusivity
λ	eddy rate
ν	kinematic viscosity
ρ	fluid density
τ	eddy time scale
ϕ	arbitrary fluid property

Subscripts

i	inner scales
j	eddy summation index
o	outer scales
p	evaluated at a location previous to an eddy event

momentum source term is $g\beta(T - T_{ref})$, where g is the magnitude of the acceleration due to gravity, β is the thermal expansion coefficient, and T_{ref} is a fixed reference temperature. For sufficiently large ΔT, this buoyant term drives the flow to a turbulent state. Positions and velocities are arranged so that x, u are wall-normal, and z, w are stream wise. The relevant nondimensional parameters for this flow include the Rayleigh number Ra which drives the flow, the Prandtl number Pr, and the Nusselt number Nu which characterizes the heat transfer across the slot, where

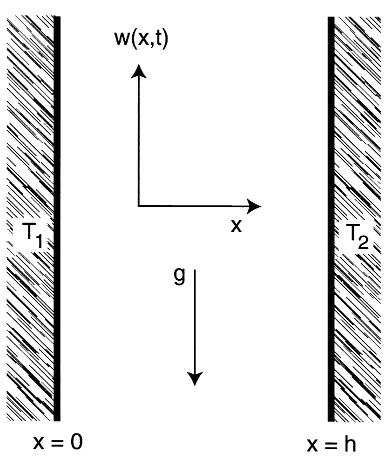

Fig. 1. Vertical slot convection.

$$Ra = \frac{g\beta\Delta T h^3}{\kappa\nu}, \tag{1}$$

$$Pr = \frac{\nu}{\kappa}, \tag{2}$$

$$Nu = \frac{q_w h}{\kappa\Delta T}. \tag{3}$$

In these expressions, ν is the kinematic viscosity, κ is the thermal diffusivity, and

$$q_w = -\kappa\left[\frac{\partial\langle T\rangle}{\partial x}\right]_w \tag{4}$$

is the wall heat flux.

3. Model description

First proposed by Kerstein [1], one-dimensional turbulence offers a conceptual departure from traditional turbulence models. Every modeling approach addresses the commonly prohibitive expense of direct computation of turbulent flows. The expense stems from the combination of two aspects: turbulence is inherently three-dimensional, and turbulence is characterized by a large range of length scales. A viable modeling approach can be based on reducing the computational burden of one or the other of these aspects. Traditional RANS, PDF, and LES models retain the three-dimensional representation of the flow, but reduce the dynamic range by modeling the small-scale phenomena. ODT takes the alternative approach: the full dynamic range of scales is represented, but only on a one-dimensional domain. Then the three-dimensional aspects of the flow are modeled. The range of flows to which ODT applies consists of those flows in which there is at most one dominant direction of spatial inhomogeneity. For the slot convection considered here, that direction is wall-normal and horizontal.

An ODT model involves instantaneous governing equations, solved on a one-dimensional domain. All processes involving molecular diffusion (viscosity, thermal diffusivity, etc.) plus source terms are represented exactly in these equations. The three-dimensional process of convection is modeled in one dimension as a series of instantaneous eddy events, as shown in Fig. 2. The size, location, and timing of these events are controlled by a probability distribution whose parameters depend on the viscosity, density, and velocity profile. It has been shown [1] that an ensemble of such eddy events reproduces the Kolmogorov spectrum in a simulation of homogeneous turbulence.

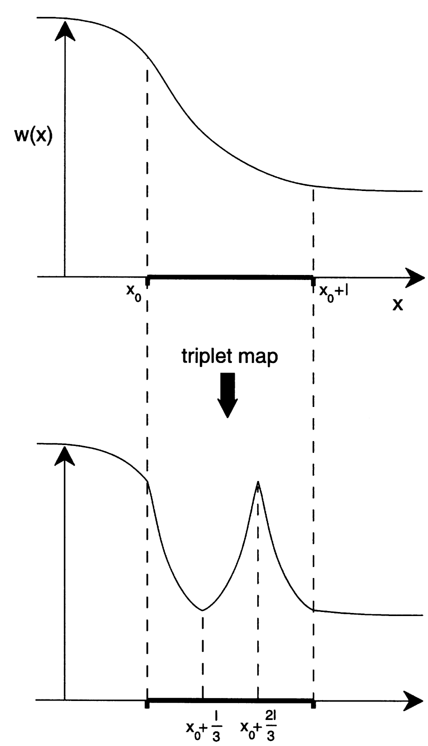

Fig. 2. The convection model: an eddy event map.

3.1. Governing equations

In the present problem, the one-dimensional domain runs horizontally from the left wall to the right wall. It is discretized in an evenly spaced grid which is resolved to the smallest scales of flow and fluid property variation. The governing equations for vertical velocity w and temperature T are

$$\frac{\partial w}{\partial t} = -\frac{1}{\rho}\frac{\partial P}{\partial z} + g\beta(T - T_{\rm ref}) + \nu\frac{\partial^2 w}{\partial x^2}, \qquad (5)$$

$$\frac{\partial T}{\partial t} = \kappa\frac{\partial^2 T}{\partial x^2}. \qquad (6)$$

In these equations, ρ is the fluid density, taken to be constant under the Boussinesq approximation. The pressure gradient term is taken to be constant over the domain, and can be expressed in terms of known quantities, depending on whether the cavity is considered open or closed. In an open cavity, the pressure gradient counterbalances the hydrostatic weight of the fluid. In this case, the pressure gradient term is set to zero, and $T_{\rm ref}$ is set to the average of the two wall temperatures. In a closed cavity, the pressure gradient term can be used to impose mass conservation on an instantaneous basis:

$$\frac{\partial}{\partial t}\int_0^h w\,{\rm d}x = 0. \qquad (7)$$

Spatial integration of Eq. (5) with this constraint gives a pressure gradient of

$$\frac{1}{\rho}\frac{\partial P}{\partial z} = g\beta\left(\bar{T} - T_{\rm ref}\right) + \frac{\nu}{h}\left[\frac{\partial w}{\partial x}\right]_0^h, \qquad (8)$$

where

$$\bar{T} = \frac{1}{h}\int_0^h T\,{\rm d}x \qquad (9)$$

is the instantaneous bulk temperature. The physical interpretation here is that the pressure gradient adjusts itself on an instantaneous basis in order to ensure that no net mass enters or leaves the infinite system — this is analogous to the solution of the Poisson equation for pressure in the Navier–Stokes equations. ODT results presented here are associated with the closed system by using Eq. (8), but with its viscous term dropped. Neglect of this term was observed to have no significant effect on the results. The velocity equation simplifies to

$$\frac{\partial w}{\partial t} = g\beta(T - \bar{T}) + \nu\frac{\partial^2 w}{\partial x^2}. \tag{10}$$

This, in conjunction with Eq. (6), specifies the governing equations.

3.2. Eddy events

Three-dimensional convection is modeled through the use of eddy events. These events are local instantaneous mappings of the spatial coordinate onto itself. Each eddy is characterized by a left endpoint x_0 and a size l. Then

$$\eta = \frac{x - x_0}{l} \tag{11}$$

defines the normalized location within the eddy, and the map $E(\eta)$ is defined by specification of its inverse, shown in Fig. 3:

$$E^{-1}(\eta) = \begin{cases} 3\eta & \text{for } 0 \le \eta < 1/3 \\ 2 - 3\eta & \text{for } 1/3 \le \eta < 2/3 \\ 3\eta - 2 & \text{for } 2/3 \le \eta < 1 \end{cases}. \tag{12}$$

The effect of the map is to modify the profile of each dependent variable for $x_0 \le x \le x_0 + l$ as shown in Fig. 2. For any flow property, we use the subscript *'p'* to denote its value just previous to the appearance of any eddy. Then the effect of an eddy on each profile is to assign

$$w(x_0 + \eta l) = w_p\left[x_0 + E^{-1}(\eta)l\right], \tag{13}$$

$$T(x_0 + \eta l) = T_p\left[x_0 + E^{-1}(\eta)l\right]. \tag{14}$$

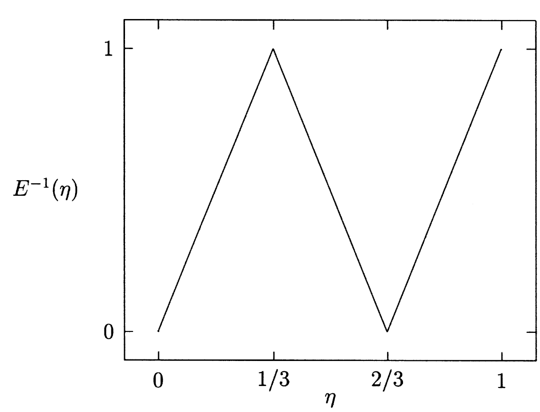

Fig. 3. Inverse eddy map $E^{-1}(\eta)$.

It follows from this formulation that for any fluid property ϕ, the expression

$$\int_{x_0}^{x_0+l} \phi \, dx \tag{15}$$

is conserved by the map. In particular, setting $\phi = 1$ for incompressible flows ensures that each eddy conserves mass.

The model specifies the timing, size, and location of each eddy by sampling from an eddy rate distribution. The number of eddies of size l and time scale τ which are expected to appear within dl of size l, within dy_0 of location y_0, and within dt of time t is $\lambda(l, \tau)\,dl\,dy_0\,dt$. The specification of the eddy rate is the same as in previous ODT implementations [3,4] in which

$$\lambda = \frac{1}{l^2\tau}, \tag{16}$$

where the time scale τ is

$$\frac{1}{\tau} = \sqrt{\left(A\left[\frac{\partial w}{\partial x}\right]_{\text{eddy}}\right)^2 - \left(\frac{16\nu}{l^2}\right)^2}, \tag{17}$$

and A is a model constant. The expression $[\partial w/\partial x]_{\text{eddy}}$ is an instantaneous velocity gradient, averaged over the length of the eddy. This eddy average is

$$\left[\frac{\partial w}{\partial x}\right]_{\text{eddy}} = \frac{2(W_R - W_L)}{l}, \tag{18}$$

with

$$W_L = \frac{2}{l}\int_{x_0}^{x_0+l/2} w(x, t)\,dx \tag{19}$$

$$W_R = \frac{2}{l}\int_{x_0+l/2}^{x_0+l} w(x, t)\,dx. \tag{20}$$

In the right-hand side of Eq. (17), the ratio of the first term to the second is the square of an eddy Reynolds number. When this Reynolds number is high, the viscous term becomes negligible and the eddy time scale becomes inversely proportional to the eddy velocity gradient. When the eddy Reynolds number is low, the viscous term increases τ and therefore diminishes the likelihood of an eddy appearance. When the expression under the square-root sign is negative, τ is set to infinity, and eddies are suppressed. The wall boundary condition of impermeability is imposed on the eddies by excluding any eddy which extends out of the domain beyond a solid wall. The constant A is set to the value $A = 0.23$, a value chosen to make ODT reproduce the wall shear stress in a boundary layer [1]. Current ODT stimulations slow that this value of A reproduces the

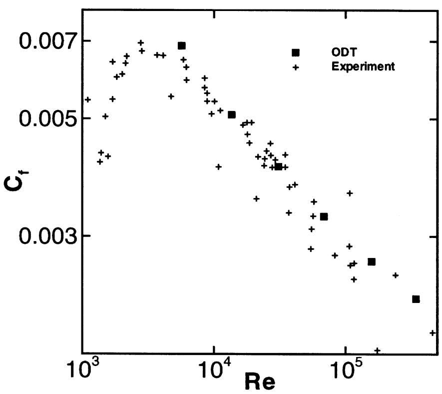

Fig. 4. Wall shear stress as a function of Reynolds number in fully-developed channel flow: ODT simulations are shown with experimental data compiled by Dean [14]. *Re* is based on the bulk velocity and channel full width; C_f is normalized by the mean centerline velocity.

shear stress for channel flow as well. Stress as a function of Reynolds number for these simulations is shown in Fig. 4.

In the model formulation of ODT, Eqs. (6), (9) and (10) evolve in continuous time, with eddies of random size and location appearing at random times, as controlled by λ in Eqs. (16)–(20). The numerical implementation of the eddy selection is described in previous work [1,4].

3.3. ODT Reynolds equations

The governing equations for mean momentum and mean temperature are derived from the ODT model using traditional control-volume analysis. For slot convection, we consider a horizontal slab over a short time increment dt which extends from the wall at the left boundary to an arbitrary point x in the domain, as shown in Fig. 5. The Reynolds decomposition for velocity and temperature is

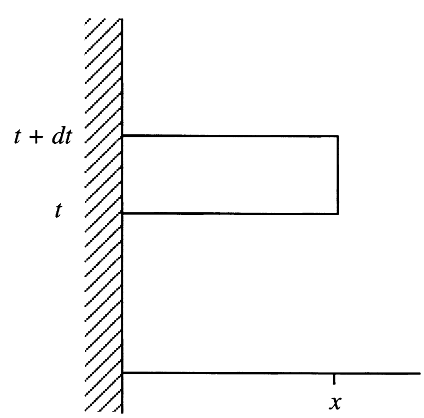

Fig. 5. Characteristic flow element.

$$w = \langle w \rangle + w', \tag{21}$$

$$T = \langle T \rangle + T', \tag{22}$$

where angle brackets denote an ensemble average. Focusing first on the momentum balance, dynamic terms are expressed per unit length in the span-wise and stream-wise directions, y and z respectively. The flow properties of the model are instantaneously homogeneous in these directions. Momentum changes in the slab by virtue of Eq. (10), and because of momentum flux across the side boundary at x due to the eddies. If $M_{\mathrm{d}t}$ is the amount of momentum per unit mass brought in by the eddies through the boundary x during time increment dt, the instantaneous balance of momentum in the slab is

$$\int_0^x \left[w(t + \mathrm{d}t) - w(t) \right] \mathrm{d}x' = g\beta \int_0^x (T - \bar{T})\, \mathrm{d}x'\, \mathrm{d}t + \nu \left[\frac{\partial w}{\partial x} \right]_0^x \mathrm{d}t + M_{\mathrm{d}t}. \tag{23}$$

The explicit connection of $M_{\mathrm{d}t}$ to the eddies is described in Appendix A. If Eq. (23) is averaged, then all of its terms become differentiable. In the limit as dt becomes small, the balance of mean momentum becomes

$$\frac{\partial}{\partial t} \int_0^x \langle w \rangle\, \mathrm{d}x' = g\beta \int_0^x \left(\langle T \rangle - \langle \bar{T} \rangle \right) \mathrm{d}x' + \nu \left[\frac{\partial \langle w \rangle}{\partial x} \right]_0^x + \frac{\partial \langle M_{\mathrm{d}t} \rangle}{\partial t}. \tag{24}$$

The last term of Eq. (24) is the ODT model for Reynolds shear stress:

$$-\langle u'w' \rangle = \frac{\partial \langle M_{\mathrm{d}t} \rangle}{\partial t}. \tag{25}$$

This assignment makes sense because of the physical correspondence between the quantity $\partial \langle M_{\mathrm{d}t} \rangle / \partial t$ and real Reynolds shear stress: In each case we have the mean rate at which vertical momentum is convected into the slab through its side boundary at x. Substituting Eq. (25) into Eq. (24) and differentiating with respect to x gives the Reynolds equation imposed by ODT:

$$\frac{\partial \langle w \rangle}{\partial t} = -\frac{\partial \langle u'w' \rangle}{\partial x} + g\beta \left(\langle T \rangle - \langle \bar{T} \rangle \right) + \nu \frac{\partial^2 \langle w \rangle}{\partial x^2}. \tag{26}$$

A similar balance of energy in the slab leads to the ODT governing equation for mean temperature:

$$\frac{\partial \langle T \rangle}{\partial t} = -\frac{\partial \langle u'T' \rangle}{\partial x} + \kappa \frac{\partial^2 \langle T \rangle}{\partial x^2}, \tag{27}$$

where the scalar flux term $-\langle u'T' \rangle$ is the mean rate at which temperature is convected into the slab through its side boundary at x.

4. ODT simulation results

The objectives here are twofold: First, we present ODT results for slot convection at the Prandtl number of air, $Pr = 0.71$, with comparison to DNS. This helps to establish which aspects ODT reproduces and which aspects it does not. Second, we show ODT at Prandtl numbers not yet investigated experimentally or with DNS to shed new light on traditional scaling arguments.

For each case, the system was driven from a quiescent flow field to a statistically stationary state by imposing the wall boundary conditions on temperature. After stationarity was reached, time averaging was used to obtain mean quantities.

4.1. Results at $Pr = 0.71$

ODT simulations of slot convection were run at the same two values of Ra as the experiments of [7]: $Ra = 8.6 \times 10^5$ and $Ra = 1.43 \times 10^6$, and at the same four values of Ra as the DNS of [5]: $Ra = 5.4 \times 10^5$, 8.2×10^5, 2.0×10^6, and 5.0×10^6. Several larger values of Ra were also run with ODT, up to about two decades beyond the highest value achieved with the DNS. Figs. 6 and 7 show ODT mean velocity and mean temperature, respectively, for the conditions of Betts and Bokhari's experiments, together with their data. Figs. 8 and 9 show back-to-back DNS comparisons of the same quantities, non-dimensionalized as in [5]. For the DNS comparisons, DNS results are shown in the left half of the slot, and ODT results are shown in the right half of the slot. Agreement with temperature profiles is good, although ODT underpredicts the heat transfer at the wall. ODT overpredicts the magnitude of the mean velocities by a consistent factor of 2, and shows curvature in the core region which is not seen in the DNS. These results reflect the fact that ODT has been formulated to be robust with respect to scalings and other parameter dependencies, despite predictive discrepancies such as those that are apparent in Figs. 6 and 8. The simplifications that cause discrepancies while preserving scaling properties are discussed in detail elsewhere [1].

ODT successfully reproduces scaling relationships of mean velocity and mean temperature found in the

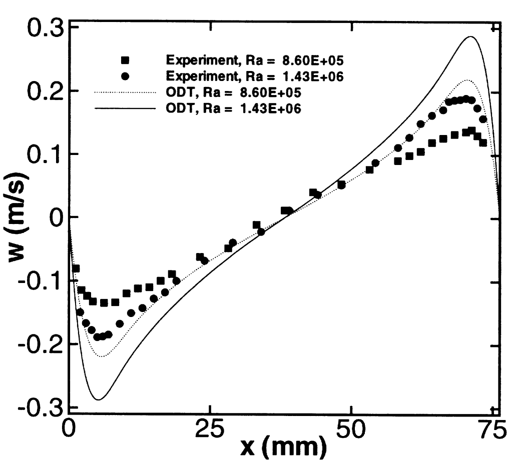

Fig. 6. Comparison of mean velocity profiles for measurements [7] and ODT.

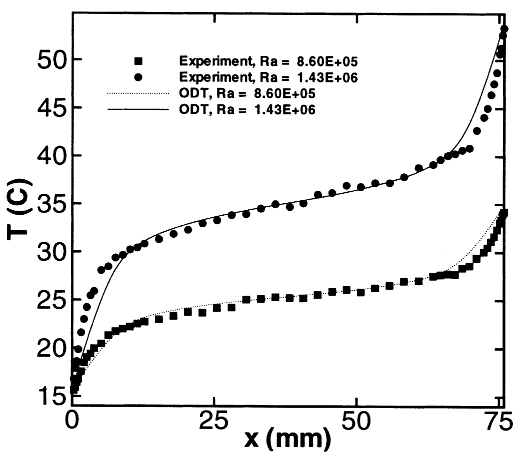

Fig. 7. Comparison of mean temperature profiles for measurements [7] and ODT.

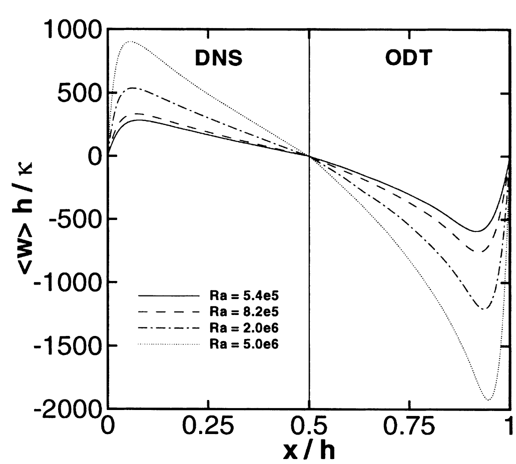

Fig. 8. Comparison of mean velocity profiles for DNS [5] and ODT.

DNS results and described in [10]. Based on the previous arguments of George and Capp [11], Nieuwstadt and Versteegh found inner scales for velocity, length, and temperature as functions of $g\beta$, q_w, and κ, but not of h, as follows:

$$w_i = (g\beta q_w \kappa)^{1/4}, \tag{28}$$

$$l_i = \kappa^{3/4} (g\beta q_w)^{-1/4}, \tag{29}$$

$$T_i = q_w^{3/4} (g\beta \kappa)^{-1/4}. \tag{30}$$

Further, they found outer scales by supposing that the velocity, length and temperature are functions of $g\beta$, q_w, and h, but not ν or κ:

$$w_o = (g\beta q_w h)^{1/3}, \tag{31}$$

$$l_o = h, \tag{32}$$

$$T_o = q_w^{2/3} (g\beta h)^{-1/3}. \tag{33}$$

The appropriateness of these scalings was tested in [10] by seeking a collapse of the results over different values of Ra. The authors reported good inner and outer collapses of temperature, poor inner collapse of mean velocity, and a marginal outer collapse of mean velocity. Figs. 10–13 show that ODT reproduces most of the scaling behavior shown in the DNS, both where collapse occurs and where it does not.

Nieuwstadt and Versteegh further examined the Ra dependence of key flow parameters, including the Nusselt number Nu, the peak mean velocity W_{max}, and the location of the peak mean velocity L_{max}. In the general scaling relationship $Nu \sim Ra^{\alpha}$, they derived the exponent value $\alpha = 1/3$ through asymptotic matching of the mean temperature profiles. Their DNS calculations of Nu showed a very good fit to the 1/3 exponent. Fig. 14 shows that ODT reproduces the 1/3 exponent. The Ra dependence of the maximum mean velocity W_{max} for ODT and DNS is shown in Fig. 15, together with inner and outer scalings of [10] and a $\sqrt{Ra}$ power law. Nieuwstadt and Versteegh derived inner and outer scaling exponents of 1/3 and 4/9, respectively, but inferred from their data that a 1/2 power law provides a better fit. ODT reproduces that 1/2 power law as well. The location L_{max} of this velocity maximum is shown for ODT and DNS in Fig. 16, together with the inner and outer scaling relations, and a closer-fitting $-1/6$ power law. Here again, ODT matches the DNS, but neither matches the derived inner and outer scaling relations. We conclude here that ODT performs es-

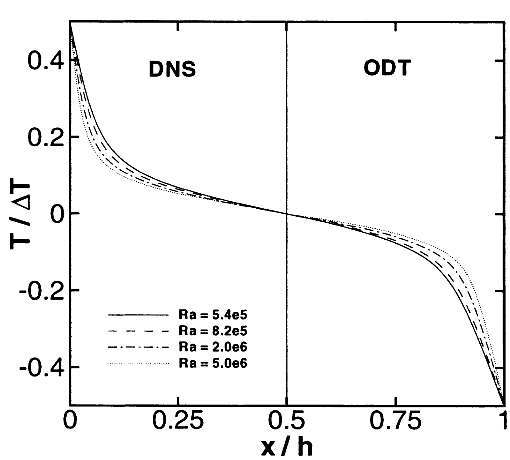

Fig. 9. Comparison of mean temperature profiles for DNS [5] and ODT.

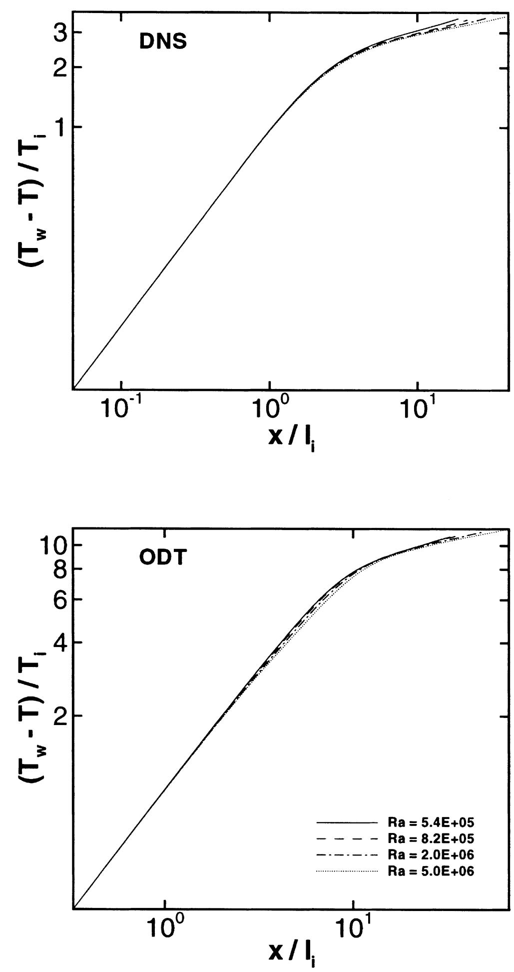

Fig. 10. Mean temperature profiles using the inner scaling of Nieuwstadt and Versteegh: comparison of ODT with DNS [5].

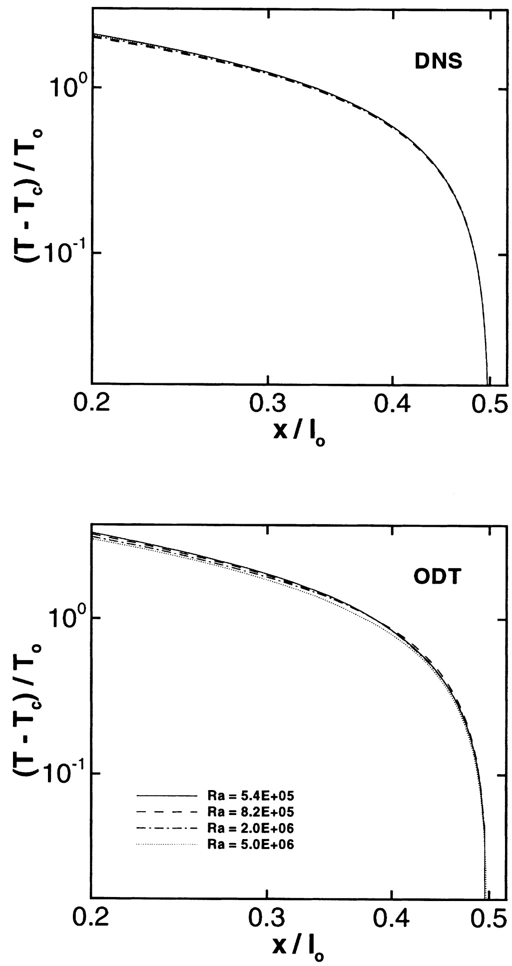

Fig. 11. Mean temperature profiles using the outer scaling of Nieuwstadt and Versteegh: comparison of ODT with DNS [5].

pecially well in its ability to match the DNS *Ra* scaling of key turbulence quantities. In each case, ODT reproduces the DNS scaling powers, independently of their consistency with theoretically derived exponents.

4.2. ODT and scaling behavior

The cost effectiveness of ODT relative to DNS enables simulations in a wider range of parameter space. In addition to raising *Ra* higher by two decades, the Prandtl number was varied in an effort to build a more comprehensive picture of the scaling behavior. Because ODT reproduces the scaling of *Nu*, W_{max}, and L_{max} as well as it does for $Pr = 0.71$, and because molecular transport is represented exactly at all scales in Eqs. (6) and (10), the scaling behavior of ODT at other values of *Pr* is likely to be a strong indication of the physical scaling behavior.

With the DNS for $Pr = 0.71$, Nieuwstadt and Versteegh were able to use scaling arguments to explain the behavior of *Nu*, but not of W_{max} or L_{max}. Using ODT over a range of Prandtl numbers, we use different scaling arguments which explain the behavior of W_{max}, but not of *Nu* or L_{max}.

Vertical slot convection has the same flow parameters as its horizontal counterpart, Rayleigh–Bénard convection. We draw from arguments for that case, which are extensively reviewed in [12]. A relatively straightforward argument [13] for the scaling of the heat transfer goes as follows: The complete list of parameters for this flow is κ, ν, $g\beta$, ΔT, and h. The physical hypothesis is then to suppose that q_w depends only on the features it can see in the near-wall region, and so the global parameter h can be crossed off the list. Under this assumption, if the walls were moved farther

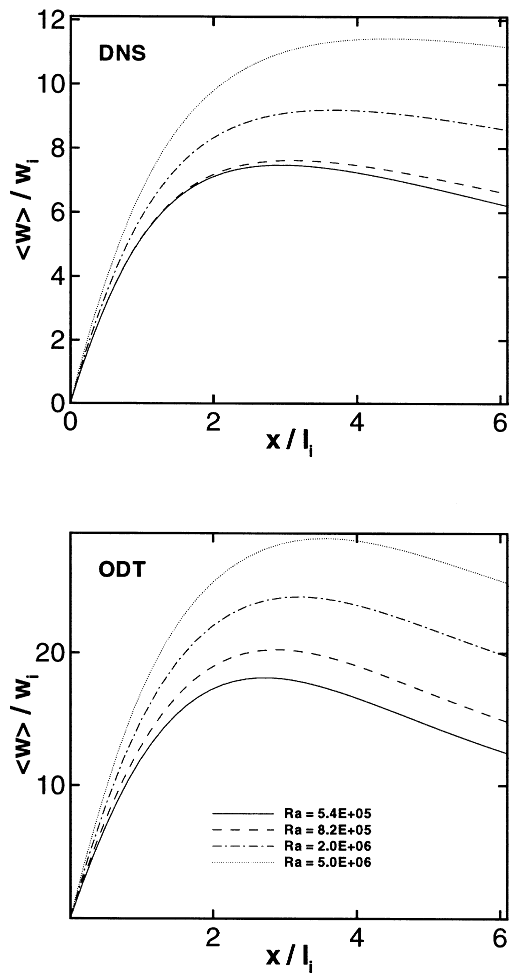

Fig. 12. Mean velocity profiles using the inner scaling of Nieuwstadt and Versteegh: comparison of ODT with DNS [5].

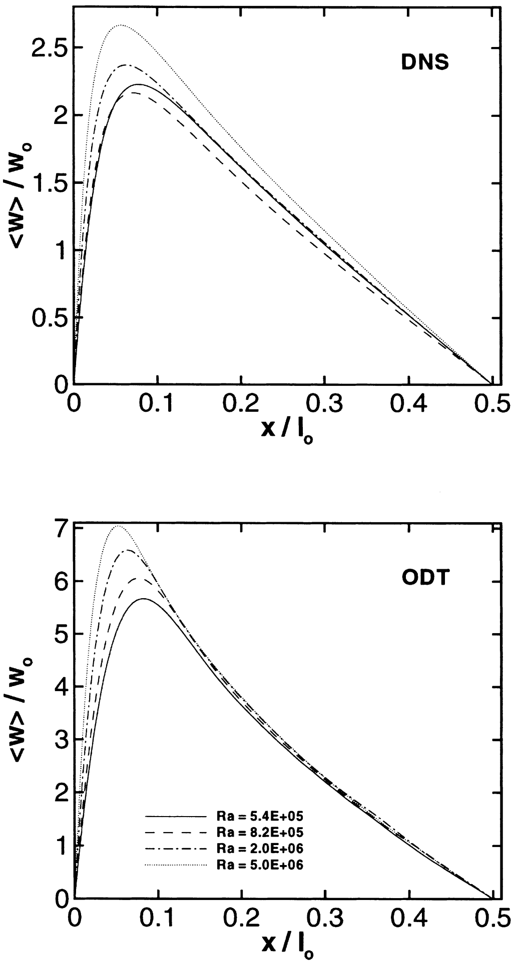

Fig. 13. Mean velocity profiles using the outer scaling of Nieuwstadt and Versteegh: comparison of ODT with DNS [5].

apart but all other physical parameters were held fixed, then the wall heat transfer would not change. It follows from this that

$$q_w = f(\kappa, \nu, g\beta, \Delta T), \tag{34}$$

where f is an unknown function. The dimensions of q_w are (length × temperature/time). The only way to form a quantity with those dimensions from a function with the arguments of Eq. (34) is to write

$$q_w \sim (g\beta\kappa)^{1/3} \Delta T^{4/3} Pr^{\alpha}, \tag{35}$$

where α is any real power. Then when we nondimensionalize q_w to form Nu, we find

$$Nu \sim Ra^{1/3}, \tag{36}$$

for any fixed Pr. This matches the scaling behavior of

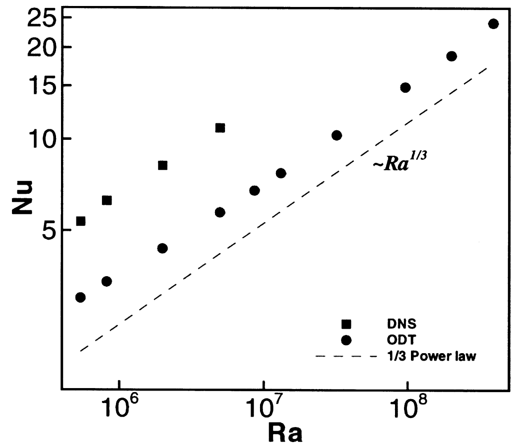

Fig. 14. Nusselt vs. Rayleigh number: comparison of DNS [5] with ODT and a cube root power law at $Pr = 0.71$.

Nu at $Pr = 0.71$ of Fig. 14, but unlike the argument of [5], it does not rely on any prior information about the mean temperature profile.

We can evaluate further how well this scaling argument applies by using ODT at different Prandtl numbers. ODT simulations of slot convection were run at a lower Prandtl number $Pr = 0.1$, for Ra ranging from 7.6×10^4 to 5.5×10^7. They were run at a higher Prandtl number $Pr = 5.0$ for Ra ranging from 3.8×10^6 to 2.7×10^9. The ODT Ra scaling of Nu at the different values of Pr is shown in Fig. 17, together with the 1/3 power law. Here we see that the Nu dependence on Ra departs from the 1/3 power law: Least squares fits to the log–log plots give scaling exponents of 0.27 and 0.44 for the low and high Pr runs, respectively. These values are taken from the

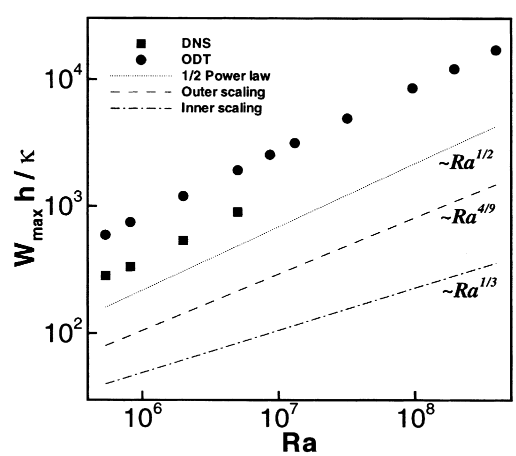

Fig. 15. Maximum mean velocity vs. Rayleigh number: comparison of DNS [5] with ODT and a square root power law at $Pr = 0.71$.

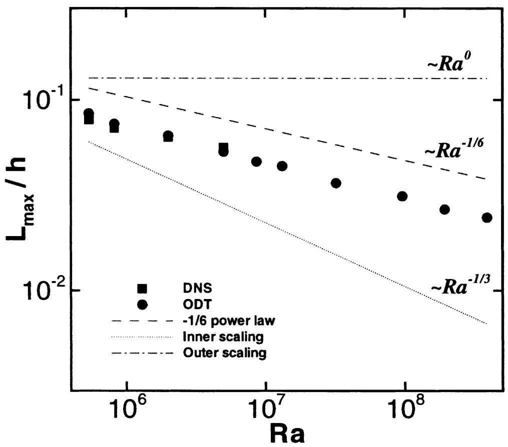

Fig. 16. Location of maximum velocity vs. Rayleigh number: comparison of DNS [5], ODT, and inner and outer scaling results at $Pr = 0.71$.

data at the six highest Rayleigh numbers in each case. This scaling behavior contradicts the relation (36), and suggests that the above scaling argument for heat transfer does not apply to slot convection in general. In particular, the wall heat transfer depends on the slot width h. The apparent lack of h dependence for $Pr = 0.71$ is fortuitous.

Somewhat more promising results for the Ra scaling of $W_{\max}$ are obtained with a similar scaling argument. If we suppose that $W_{\max}$ can be expressed as a function of $g\beta$, ΔT, and h, but not of molecular properties κ or ν, then dimensional analysis imposes the result

$$\frac{W_{\max}h}{\kappa} \sim (Ra\,Pr)^{1/2}. \quad (37)$$

For fixed Pr, Eq. (37) reduces to

$$\frac{W_{\max}h}{\kappa} \sim Ra^{1/2}. \quad (38)$$

This matches both the ODT and DNS scaling at $Pr = 0.71$ shown in Fig. 15. The 1/2 exponent was not found by Nieuwstadt and Versteegh [10] because they characterized the temperature dependence with q_w, rather than ΔT, for consistency with their asymptotic profile matching. While the present scaling argument sacrifices such consistency, it provides a strong suggestion that the maximum mean velocity is a globally determined quantity, and does not depend on molecular transport. Fig. 18 shows the scaling of $W_{\max}$ based on ODT results for three different Pr values. The close agreement with the 1/2 exponent for all cases suggests that this scaling behavior of $W_{\max}$ is a robust result. The scaling hypothesis that $W_{\max}$ is independent of molecular properties κ and ν is further tested in Fig. 19: Under such independence, a plot of $W_{\max}h/\kappa$ versus the product $Ra\,Pr$ should collapse to a single line of slope 1/2 on a log–log plot, as given by Eq. (37). The lack of complete collapse shows a weak Prandtl number dependence of $W_{\max}$.

The location $L_{\max}$ of the peak mean velocity is plotted as a function of Ra for the three different values of Pr in Fig. 20. Although the $-1/6$ power law is a good fit for all the cases, it continues to defy any scaling argument.

Although the use of ΔT as a scaling parameter has been shown [5] to be inconsistent with known features of the mean temperature, we find that it works well for the scaling of the peak mean velocity. Because of this and the unexplained scaling of $L_{\max}$, no comprehensive, systematic scaling interpretation is apparent for this flow.

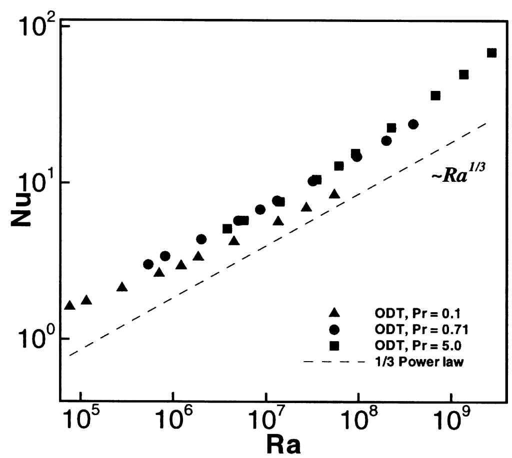

Fig. 17. ODT Nu scaling at different values of Pr, compared with the 1/3 power law.

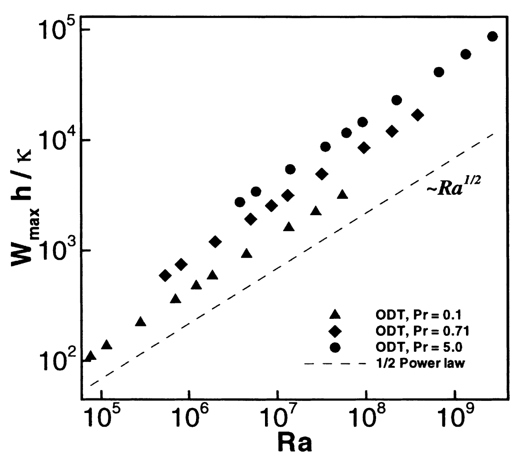

Fig. 18. ODT $W_{\max}h/k$ scaling at different values of Pr, compared with the 1/2 power law.

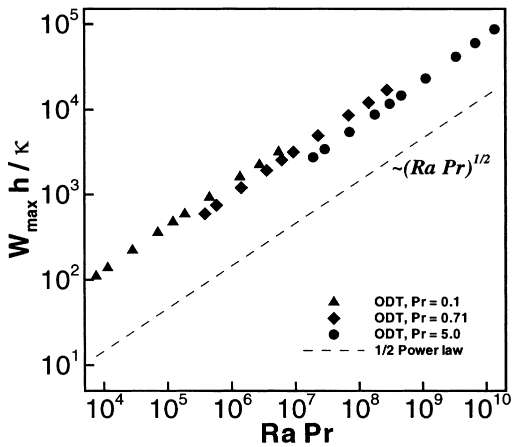

Fig. 19. ODT $W_{\max}h/\kappa$ scaling at different values of $Ra\ Pr$, compared with the 1/2 power law.

5. Conclusion

ODT is used here to simulate the buoyant convection which is driven by an imposed temperature difference across two vertical walls. Additional modeling terms are restricted to the addition of a buoyant source term in the velocity equation, using the Boussinesq approximation. No empirical constants are added to the model to accommodate this flow; the value of the constant A in the eddy-rate expression is set to 0.23, which is identical to the value used in previous wall-bounded flow simulations.

Comparisons with DNS data show that ODT reproduces much of the scaling behavior of the flow which is seen at $Pr = 0.71$. Within a constant factor, ODT reproduces the Ra dependence of the heat transfer, maximum mean velocity, and its location. ODT is used

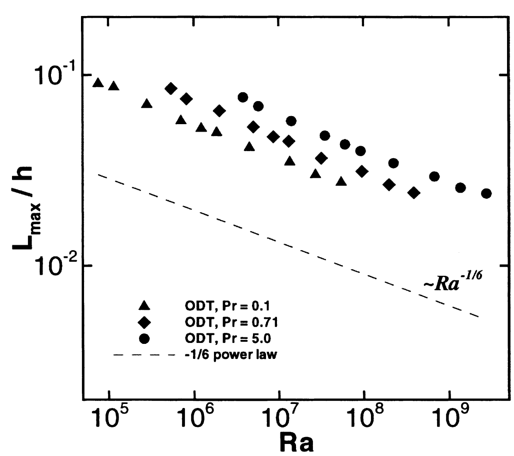

Fig. 20. ODT $L_{\max}/h$ scaling at different values of Pr, compared with the $-1/6$ power law.

to further explore the scaling behavior by simulating the flow at different Prandtl numbers. ODT results suggest that the scaling $Nu \sim Ra^{1/3}$ applies only to the case in which $Pr = 0.71$, and therefore that the heat transfer depends on the wall separation in general. Results also suggest that the maximum mean velocity scales as $\sqrt{Ra}$ over a range of Prandtl numbers, consistent with a simple argument in which the molecular properties play a minimal role. These results suggest that it would be fruitful to run DNS or experiments of this flow configuration at different Prandtl numbers to see if these relations carry over to real flows.

Acknowledgements

We wish to thank Prof. F. T. M. Nieuwstadt and Dr. T. A. M. Versteegh for providing us with their DNS data of [5], and Dr. P. L. Betts for providing us with the experimental data of [7]. This work was supported by the U. S. Department of Energy, through Sandia National Laboratories' Laboratory Directed Research and Development Program.

Appendix A. ODT eddy-based flux

Fluxes of quantities can be written explicitly in terms of the instantaneous profiles and the eddy map of Eq. (12) and Fig. 3. We are interested in the net transfer of an arbitrary property ϕ by the eddies into the slab of Fig. 5 through the right-side boundary at location x. Suppose the jth eddy has left endpoint $x_{0,j}$, size l_j, and occurs at time t_j. Let x' be a dummy variable which traverses the length of the eddy, just after the eddy has occurred. Let $\mathrm{d}Q_j$ be the net change of $\int_0^x \phi(\hat{x})\,\mathrm{d}\hat{x}$ caused by eddy-induced transfer of ϕ into the small volume within $\mathrm{d}x'$ of x'. We need to know where this volume was before the eddy occurred. This previous location is

$$x_{p,j} = l_j E^{-1}\left(\frac{x' - x_{0,j}}{l_j}\right) + x_{0,j}, \tag{A1}$$

where E^{-1} is the inverse eddy triplet map given by Eq. (12). Then we have

$$\mathrm{d}Q_j = \left[H(x - x') - H(x - x_{p,j})\right]\phi(x_{p,j}, t_j)\,\mathrm{d}x', \tag{A2}$$

where the expression with Heaviside functions in the square brackets is 1 if the fluid at x' has crossed into the slab, -1 if the fluid at x' has crossed out of the slab, and zero if it has not crossed x in either direction. The non-local behavior of ODT is brought out in Eq. (A2): the stuff crossing location x was previously at location $x_{p,j}$ given by Eq. (A1), and $x_{p,j}$ does not approach x in the limit as $dt \to 0$ or as $dx' \to 0$. If a total of n_t eddies appear within $dt/2$ of time t, then the net amount of ϕ brought into the slab is determined by integrating Eq. (A2) over the eddy, and then summing over all n_t eddies:

$$Q_{dt} = \sum_{j=1}^{n_t} \int_{x_{0,j}}^{x_{0,j}+l_j} \Big[H(x - x') - H(x - x_{p,j}) \Big] \times \phi(x_{p,j}, t_j)\, dx' \tag{A3}$$

For the case where ϕ is the velocity w, this Q_{dt} is M_{dt} of Eq. (23). Turbulent fluxes are then obtained by averaging Eq. (A3) and differentiating with respect to time, in that order. For the velocity and temperature in the flow considered here, we have

$$-\langle u'w' \rangle = \frac{\partial}{\partial t} \left\langle \sum_{j=1}^{n_t} \int_{x_{0,j}}^{x_{0,j}+l_j} \Big[H(x - x') - H(x - x_{p,j}) \Big] w(x_{p,j}, t_j)\, dx' \right\rangle, \tag{A4}$$

$$-\langle u'T' \rangle = \frac{\partial}{\partial t} \left\langle \sum_{j=1}^{n_t} \int_{x_{0,j}}^{x_{0,j}+l_j} \Big[H(x - x') - H(x - x_{p,j}) \Big] T(x_{p,j}, t_j)\, dx' \right\rangle. \tag{A5}$$

References

[1] A.R. Kerstein, One-dimensional turbulence: model formulation and application to homogeneous turbulence, shear flows, and buoyant stratified flows, Journal of Fluid Mechanics 392 (1999) 277–334.

[2] A.R. Kerstein, One-dimensional turbulence. Part 2: Staircases in double-diffusive convection, Dynamics of Atmospheres and Oceans 30 (1999) 25–46.

[3] A.R. Kerstein, T.D. Dreeben, Prediction of turbulent free shear flow statistics using a simple stochastic model, Physics of Fluids 12 (2000) 418–424.

[4] T. Echekki, A.R. Kerstein, J.Y. Chen, T.D. Dreeben, 'One-dimensional turbulence' simulation of turbulent jet diffusion flames: model formulation and illustrative applications, Combustion and Flame, submitted.

[5] T.A.M. Versteegh, F.T.M. Nieuwstadt, A direct numerical simulation of natural convection between two infinite vertical differentially heated walls; scaling laws and wall functions, International Journal of Heat and Mass Transfer 42 (1999) 3673–3693.

[6] A.A. Dafa'Alla, P.L. Betts, Experimental study of turbulent natural convection in a tall air cavity, Experimental Heat Transfer 9 (1996) 165–194.

[7] P.L. Betts, I.H. Bokhari, Experiments on turbulent natural convection of air in a tall cavity, in: Fifth ERCOFTAC workshop on refined flow modelling, Chatou, France, 1996.

[8] R. Boudjemadi, V. Maupu, D. Laurence, P. Le Quéré, Budgets of turbulent stresses and fluxes in a vertical slot natural convection flow at $Ra = 10^5$ and 5.4×10^5, International Journal of Heat and Fluid Flow 18 (1997) 70–79.

[9] Z. Warhaft, Passive scalars in turbulent flows, Annual Review of Fluid Mechanics 32 (2000) 203–240.

[10] F.T.M. Nieuwstadt, T.A.M. Versteegh, DNS of natural convection between two vertical differentially heated walls, in: Eleventh Symposium on Turbulent Shear Flows, Grenoble, France, 1997.

[11] W.K. George, S.P. Capp, A theory for natural convection turbulent boundary layers next to heated vertical surfaces, International Journal of Heat and Mass Transfer 22 (1979) 813–826.

[12] E.D. Siggia, High Rayleigh number convection, Annual Review of Fluid Mechanics 26 (1994) 137–168.

[13] E.A. Spiegel, Convection in stars, Annual Review of Astronomy and Astrophysics 9 (1971) 323–352.

[14] R.B. Dean, Reynolds number dependence of skin friction and other bulk flow variables in two-dimensional rectangular duct flow, Journal of Fluids Engineering 100 (1978) 215–223.